

World Journal of *Gastroenterology*

World J Gastroenterol 2022 August 21; 28(31): 4235-5110



REVIEW

- 4235 Early diagnosis of pancreatic cancer: What strategies to avoid a foretold catastrophe
Tonini V, Zanni M
- 4249 Insights into induction of the immune response by the hepatitis B vaccine
Di Lello FA, Martínez AP, Flichman DM
- 4263 Evidence-based pathogenesis and treatment of ulcerative colitis: A causal role for colonic epithelial hydrogen peroxide
Pravda J

MINIREVIEWS

- 4299 Recent advances in multidisciplinary therapy for adenocarcinoma of the esophagus and esophagogastric junction
Zheng YH, Zhao EH

ORIGINAL ARTICLE**Basic Study**

- 4310 Exosomal glypican-1 is elevated in pancreatic cancer precursors and can signal genetic predisposition in the absence of endoscopic ultrasound abnormalities
Moutinho-Ribeiro P, Batista IA, Quintas ST, Adem B, Silva M, Morais R, Peixoto A, Coelho R, Costa-Moreira P, Medas R, Lopes S, Vilas-Boas F, Baptista M, Dias-Silva D, Esteves AL, Martins F, Lopes J, Barroca H, Carneiro F, Macedo G, Melo SA
- 4328 Duodenal-jejunal bypass reduces serum ceramides *via* inhibiting intestinal bile acid-farnesoid X receptor pathway
Cheng ZQ, Liu TM, Ren PF, Chen C, Wang YL, Dai Y, Zhang X
- 4338 Duodenal-jejunal bypass increases intraduodenal bile acids and upregulates duodenal SIRT1 expression in high-fat diet and streptozotocin-induced diabetic rats
Han HF, Liu SZ, Zhang X, Wei M, Huang X, Yu WB

Retrospective Study

- 4351 Approaches to reconstruction of inferior vena cava by *ex vivo* liver resection and autotransplantation in 114 patients with hepatic alveolar echinococcosis
Maimaitinijati Y, Aji T, Jiang TM, Ran B, Shao YM, Zhang RQ, Guo Q, Wang ML, Wen H
- 4363 Application of computed tomography-based radiomics in differential diagnosis of adenocarcinoma and squamous cell carcinoma at the esophagogastric junction
Du KP, Huang WP, Liu SY, Chen YJ, Li LM, Liu XN, Han YJ, Zhou Y, Liu CC, Gao JB

- 4376 Preoperative contrast-enhanced computed tomography-based radiomics model for overall survival prediction in hepatocellular carcinoma

Deng PZ, Zhao BG, Huang XH, Xu TF, Chen ZJ, Wei QF, Liu XY, Guo YQ, Yuan SG, Liao WJ

- 4390 Nationwide retrospective study of hepatitis B virological response and liver stiffness improvement in 465 patients on nucleos(t)ide analogue

Ramji A, Doucette K, Cooper C, Minuk GY, Ma M, Wong A, Wong D, Tam E, Conway B, Truong D, Wong P, Barrett L, Ko HH, Haylock-Jacobs S, Patel N, Kaplan GG, Fung S, Coffin CS

Observational Study

- 4399 Radiomics and nomogram of magnetic resonance imaging for preoperative prediction of microvascular invasion in small hepatocellular carcinoma

Chen YD, Zhang L, Zhou ZP, Lin B, Jiang ZJ, Tang C, Dang YW, Xia YW, Song B, Long LL

- 4417 Prevalence and clinical characteristics of autoimmune liver disease in hospitalized patients with cirrhosis and acute decompensation in China

Shen ZX, Wu DD, Xia J, Wang XB, Zheng X, Huang Y, Li BL, Meng ZJ, Gao YH, Qian ZP, Liu F, Lu XB, Shang J, Yan HD, Zheng YB, Gu WY, Zhang Y, Wei JY, Tan WT, Hou YX, Zhang Q, Xiong Y, Zou CC, Chen J, Huang ZB, Jiang XH, Luo S, Chen YY, Gao N, Liu CY, Yuan W, Mei X, Li J, Li T, Zhou XY, Deng GH, Chen JJ, Ma X, Li H

- 4431 Simple cholecystectomy is an adequate treatment for grade I T1bN0M0 gallbladder carcinoma: Evidence from 528 patients

Shao J, Lu HC, Wu LQ, Lei J, Yuan RF, Shao JH

META-ANALYSIS

- 4442 Current standard values of health utility scores for evaluating cost-effectiveness in liver disease: A meta-analysis

Ishinuki T, Ota S, Harada K, Kawamoto M, Meguro M, Kutomi G, Tatsumi H, Harada K, Miyanishi K, Kato T, Ohyanagi T, Hui TT, Mizuguchi T

CASE REPORT

- 4456 Low-grade myofibroblastic sarcoma of the liver misdiagnosed as cystadenoma: A case report

Li J, Huang XY, Zhang B

LETTER TO THE EDITOR

- 4463 Evidence-based considerations on bowel preparation for colonoscopy

Argyriou K, Parra-Blanco A

- 4467 Influence of different portal vein branches on hepatic encephalopathy during intrahepatic portal shunt *via* jugular vein

Yao X, He S, Wei M, Qin JP

- 4471 Promising role of D-amino acids in irritable bowel syndrome

Ikeda Y, Taniguchi K, Sawamura H, Tsuji A, Matsuda S

REVIEW

- 5093** Robotic, self-propelled, self-steerable, and disposable colonoscopes: Reality or pipe dream? A state of the art review

Winters C, Subramanian V, Valdastrì P

ABOUT COVER

Editorial Board Member of *World Journal of Gastroenterology*, Mortada H F El-Shabrawi, MD, FAASLD, Professor, Department of Paediatrics, Kasr Alainy School of Medicine, Cairo University, Cairo 11562, Egypt. melshabrawi@kasralainy.edu.eg

AIMS AND SCOPE

The primary aim of *World Journal of Gastroenterology* (*WJG, World J Gastroenterol*) is to provide scholars and readers from various fields of gastroenterology and hepatology with a platform to publish high-quality basic and clinical research articles and communicate their research findings online. *WJG* mainly publishes articles reporting research results and findings obtained in the field of gastroenterology and hepatology and covering a wide range of topics including gastroenterology, hepatology, gastrointestinal endoscopy, gastrointestinal surgery, gastrointestinal oncology, and pediatric gastroenterology.

INDEXING/ABSTRACTING

The *WJG* is now abstracted and indexed in Science Citation Index Expanded (SCIE, also known as SciSearch®), Current Contents/Clinical Medicine, Journal Citation Reports, Index Medicus, MEDLINE, PubMed, PubMed Central, Scopus, Reference Citation Analysis, China National Knowledge Infrastructure, China Science and Technology Journal Database, and Superstar Journals Database. The 2022 edition of Journal Citation Reports® cites the 2021 impact factor (IF) for *WJG* as 5.374; IF without journal self cites: 5.187; 5-year IF: 5.715; Journal Citation Indicator: 0.84; Ranking: 31 among 93 journals in gastroenterology and hepatology; and Quartile category: Q2. The *WJG*'s CiteScore for 2021 is 8.1 and Scopus CiteScore rank 2021: Gastroenterology is 18/149.

RESPONSIBLE EDITORS FOR THIS ISSUE

Production Editor: Yi-Xuan Cai; Production Department Director: Xiang Li; Editorial Office Director: Jia-Ru Fan.

NAME OF JOURNAL

World Journal of Gastroenterology

ISSN

ISSN 1007-9327 (print) ISSN 2219-2840 (online)

LAUNCH DATE

October 1, 1995

FREQUENCY

Weekly

EDITORS-IN-CHIEF

Andrzej S Tarnawski

EDITORIAL BOARD MEMBERS

<http://www.wjgnet.com/1007-9327/editorialboard.htm>

PUBLICATION DATE

August 21, 2022

COPYRIGHT

© 2022 Baishideng Publishing Group Inc

INSTRUCTIONS TO AUTHORS

<https://www.wjgnet.com/bpg/gerinfo/204>

GUIDELINES FOR ETHICS DOCUMENTS

<https://www.wjgnet.com/bpg/GerInfo/287>

GUIDELINES FOR NON-NATIVE SPEAKERS OF ENGLISH

<https://www.wjgnet.com/bpg/gerinfo/240>

PUBLICATION ETHICS

<https://www.wjgnet.com/bpg/GerInfo/288>

PUBLICATION MISCONDUCT

<https://www.wjgnet.com/bpg/gerinfo/208>

ARTICLE PROCESSING CHARGE

<https://www.wjgnet.com/bpg/gerinfo/242>

STEPS FOR SUBMITTING MANUSCRIPTS

<https://www.wjgnet.com/bpg/GerInfo/239>

ONLINE SUBMISSION

<https://www.f6publishing.com>

Observational Study

Radiomics and nomogram of magnetic resonance imaging for preoperative prediction of microvascular invasion in small hepatocellular carcinoma

Yi-Di Chen, Ling Zhang, Zhi-Peng Zhou, Bin Lin, Zi-Jian Jiang, Cheng Tang, Yi-Wu Dang, Yu-Wei Xia, Bin Song, Li-Ling Long

Specialty type: Gastroenterology and hepatology

Provenance and peer review:

Unsolicited article; Externally peer reviewed.

Peer-review model: Single blind

Peer-review report's scientific quality classification

Grade A (Excellent): A
Grade B (Very good): 0
Grade C (Good): C
Grade D (Fair): 0
Grade E (Poor): 0

P-Reviewer: Granito A, Italy;
Hussein R, Egypt

Received: December 14, 2021

Peer-review started: December 14, 2021

First decision: January 27, 2022

Revised: February 5, 2022

Accepted: July 24, 2022

Article in press: July 24, 2022

Published online: August 21, 2022



Yi-Di Chen, Ling Zhang, Zi-Jian Jiang, Cheng Tang, Li-Ling Long, Department of Radiology, The First Affiliated Hospital of Guangxi Medical University, Nanning 530021, Guangxi Zhuang Autonomous Region, China

Zhi-Peng Zhou, Bin Lin, Department of Radiology, Affiliated Hospital of Guilin Medical University, Guilin 541001, Guangxi Zhuang Autonomous Region, China

Yi-Wu Dang, Department of Pathology, The First Affiliated Hospital of Guangxi Medical University, Nanning 5350021, Guangxi Zhuang Autonomous Region, China

Yu-Wei Xia, Department of Technology, Huiying Medical Technology (Beijing), Beijing 100192, China

Bin Song, Department of Radiology, West China Hospital, Sichuan University, Chengdu 610041, Sichuan Province, China

Li-Ling Long, Key Laboratory of Early Prevention and Treatment for Regional High Frequency Tumor, Ministry of Education, Guangxi Medical University, Nanning 530021, Guangxi Zhuang Autonomous Region, China

Li-Ling Long, Guangxi Key Laboratory of Immunology and Metabolism for Liver Diseases, First Affiliated Hospital of Guangxi Medical University, Nanning 530021, Guangxi Zhuang Autonomous Region, China

Corresponding author: Li-Ling Long, MD, Chairman, Chief Doctor, Professor, Department of Radiology, The First Affiliated Hospital of Guangxi Medical University, No. 6 Shuangyong Road, Nanning 530021, Guangxi Zhuang Autonomous Region, China.
cjr.longliling@vip.163.com

Abstract

BACKGROUND

Microvascular invasion (MVI) of small hepatocellular carcinoma (sHCC) (≤ 3.0 cm) is an independent prognostic factor for poor progression-free and overall survival. Radiomics can help extract imaging information associated with tumor pathophysiology.

AIM

To develop and validate radiomics scores and a nomogram of gadolinium ethoxybenzyl-diethyl-enetriamine pentaacetic acid (Gd-EOB-DTPA)-enhanced magnetic resonance imaging (MRI) for preoperative prediction of MVI in sHCC.

METHODS

In total, 415 patients were diagnosed with sHCC by postoperative pathology. A total of 221 patients were retrospectively included from our hospital. In addition, we recruited 94 and 100 participants as independent external validation sets from two other hospitals. Radiomics models of Gd-EOB-DTPA-enhanced MRI and diffusion-weighted imaging (DWI) were constructed and validated using machine learning. As presented in the radiomics nomogram, a prediction model was developed using multivariable logistic regression analysis, which included radiomics scores, radiologic features, and clinical features, such as the alpha-fetoprotein (AFP) level. The calibration, decision-making curve, and clinical usefulness of the radiomics nomogram were analyzed. The radiomic nomogram was validated using independent external cohort data. The areas under the receiver operating curve (AUC) were used to assess the predictive capability.

RESULTS

Pathological examination confirmed MVI in 64 (28.9%), 22 (23.4%), and 16 (16.0%) of the 221, 94, and 100 patients, respectively. AFP, tumor size, non-smooth tumor margin, incomplete capsule, and peritumoral hypointensity in hepatobiliary phase (HBP) images had poor diagnostic value for MVI of sHCC. Quantitative radiomic features (1409) of MRI scans were extracted. The classifier of logistic regression (LR) was the best machine learning method, and the radiomics scores of HBP and DWI had great diagnostic efficiency for the prediction of MVI in both the testing set (hospital A) and validation set (hospital B, C). The AUC of HBP was 0.979, 0.970, and 0.803, respectively, and the AUC of DWI was 0.971, 0.816, and 0.801 ($P < 0.05$), respectively. Good calibration and discrimination of the radiomics and clinical combined nomogram model were exhibited in the testing and two external validation cohorts (C-index of HBP and DWI were 0.971, 0.912, 0.808, and 0.970, 0.843, 0.869, respectively). The clinical usefulness of the nomogram was further confirmed using decision curve analysis.

CONCLUSION

AFP and conventional Gd-EOB-DTPA-enhanced MRI features have poor diagnostic accuracies for MVI in patients with sHCC. Machine learning with an LR classifier yielded the best radiomics score for HBP and DWI. The radiomics nomogram developed as a noninvasive preoperative prediction method showed favorable predictive accuracy for evaluating MVI in sHCC.

Key Words: Magnetic resonance imaging; Hepatocellular carcinoma; Radiomics; Nomogram

©The Author(s) 2022. Published by Baishideng Publishing Group Inc. All rights reserved.

Core Tip: Microvascular invasion (MVI) accounts for approximately 20% of small hepatocellular carcinoma (sHCC) (≤ 3.0 cm) and is a poor independent prognostic factor for progression-free survival and overall survival. However, no studies have been published on the preoperative prediction of the MVI of sHCC. This multi-center study was developed and validated radiomics scores and nomogram of gadoxetic acid-enhanced magnetic resonance imaging (EOB-MRI) for the preoperative prediction of MVI in sHCC. The results demonstrated that AFP and conventional EOB-MRI features have poor diagnostic accuracy for MVI in patients with sHCC. The radiomics scores of HBP and diffusion-weighted imaging can improve the ability to predict MVI. As a noninvasive preoperative prediction method, the radiomics nomogram presented in this study showed a favorable predictive accuracy in evaluating MVI of sHCC, which may help reassess the clinical therapeutic regimen for patients with sHCC.

Citation: Chen YD, Zhang L, Zhou ZP, Lin B, Jiang ZJ, Tang C, Dang YW, Xia YW, Song B, Long LL. Radiomics and nomogram of magnetic resonance imaging for preoperative prediction of microvascular invasion in small hepatocellular carcinoma. *World J Gastroenterol* 2022; 28(31): 4399-4416

URL: <https://www.wjgnet.com/1007-9327/full/v28/i31/4399.htm>

DOI: <https://dx.doi.org/10.3748/wjg.v28.i31.4399>

INTRODUCTION

Hepatocellular carcinoma (HCC) is the fourth most common cause of cancer-related death and ranks sixth in terms of incident cases worldwide[1]. HCC is an important public health problem worldwide, and the death rate has increased over the past few years[2,3]. The cut-off size to define small HCC (sHCC) has been adopted as 3.0 cm[4]. Although the prognosis of sHCC is better than other types of HCC, the higher postoperative recurrence rate results in poor long-term outcomes after resection of sHCC[5]. Previous studies have confirmed that tumor size, higher tumor stage, worse histological differentiation, and the presence of microvascular invasion (MVI) are significant risk factors for short-term recurrence of HCC[6-8]. In particular, the incidence of MVI, which is an independent poor prognostic factor for progression-free survival and overall survival of patients with sHCC, is generally about 20% in sHCC[9]. The presence or absence of MVI also suggests the need for different therapeutic options for HCC. Research has indicated that transcatheter arterial chemoembolization combined with intensity-modulated radiotherapy and sorafenib showed obvious clinical benefits in HCC patients with MVI[10]. Enlarged hepatectomy may be necessary for patients with sHCC and MVI.

Pathological examination of postoperative specimens is the gold standard for the diagnosis of MVI [11]. However, postoperative specimens exhibit hysteresis, which is not ideal for guiding treatment. In addition to being an invasive method, biopsy carries some risks of bleeding or tumor seeding[12]. Gadolinium ethoxybenzyl-diethylenetriamine pentaacetic acid (Gd-EOB-DTPA) contrast-enhanced liver magnetic resonance imaging (MRI) is a noninvasive examination used to diagnose a variety of liver diseases[13] and can be used to assess liver function in patients with various stages of liver disease[14]. Gd-EOB-DTPA MRI has been used to predict MVI based on tumor size, non-smooth tumor margin, incomplete capsule, and peritumoral hypointensity in the hepatobiliary phase[15-18]. However, sHCC has a small size, regular margin, complete capsule (or no capsule), and is usually free of peritumoral hypointensity. Therefore, it is difficult to predict the MVI of sHCC using traditional GD-EOB-DTPA MRI features.

Radiomics is an emerging field that attempts to quantify tumor heterogeneity related to the tumor parenchyma and microenvironment, including cellularity, extracellular matrix deposition, angiogenesis, necrosis, and fibrosis[19,20]. Machine learning is a scientific method of algorithms and statistical models that uses computers to interpret or predict patterns and inferences[21]. In many medical situations, medical imaging can be analyzed by machine learning through a series of processes, such as image registration, image segmentation, object detection, classification, and outcome prediction[22,23]. Automated computer algorithms can be used for quantitative image analysis, which can objectively quantify the heterogeneity of an image by measuring the spatial variation in the pixel intensity[24]. Radiomics with quantitative analysis provides a potential method for the diagnosis and prognosis of cancers[25,26]. Although a few studies have explored the feasibility of using radiomics based on computed tomography (CT) or MRI features to predict MVI in HCC[27-29], to our knowledge, previous studies have not investigated the prediction of MVI in sHCC. Therefore, this study aimed to explore the diagnostic value of liver Gd-EOB-DTPA MRI features in MVI of sHCC and to construct and validate the predictive efficacy of radiomics signatures and a nomogram for MVI in sHCC. This study also aimed to confirm the best modeling sequences, including images of T1 weighted imaging (T1WI), T2 weighted imaging (T2WI), diffusion-weighted imaging (DWI), and post-Gd-EOB-DTPA enhancement images of the arterial phase (AP), portal vein phase (PVP), and hepatobiliary phase (HBP), for extracting radiomics signatures by machine learning.

MATERIALS AND METHODS

Study cohort

The ethical review board of our institution approved this multi-center and external validation study (No. 2019 KY-E-134). This study adhered to the principles of the Declaration of Helsinki and the requirement for informed consent was waived. First, we retrospectively searched our institution's (Guangxi Medical University First Affiliated Hospital, Hospital A) departmental electronic database for patients with consecutive hospital visits who had undergone upper-abdomen MRI between January 2016 and June 2020. A total of 221 patients were enrolled who met the following inclusion criteria: (1) Patients received Gd-EOB-DTPA enhanced upper-abdomen MRI and small HCC (tumor size \leq 3.0 cm) were diagnosed; (2) no macrovascular tumor invasion on MRI (*i.e.*, no tumor thrombus in the hepatic or portal veins); (3) primary HCC were diagnosed by histopathologic examination within two weeks after the MRI examination; and (4) MR images were of sufficient image quality. The exclusion criteria of this study were: (1) Patients who had undergone previous hepatobiliary surgery or liver-directed therapy (*i.e.*, transarterial chemoembolization or ablation); and (2) the lesions were diagnosed other than primary HCC. Second, we continuously recruited 94 and 100 participants as independent external validation sets from two other hospitals (Affiliated Hospital of Guilin Medical University and West China Hospital, Hospital B and C) between July 2020 and August 2021 using the same inclusion and exclusion criteria. All patients underwent hepatectomy and pathologic assessment within two weeks of the MRI

examination. The alpha fetal protein (AFP), Child-Pugh grades (grade A to C), and model for end-stage liver disease (MELD) scores were also analyzed and calculated for all patients (Figure 1).

Histopathologic analysis

Two experienced pathologists performed all the histological analyses in our central pathology laboratory. The Edmondson-Steiner classification was used to identify the major histological grades of HCC. When a tumor within a vascular space was lined by the endothelium, MVI was confirmed to be visible only microscopically, and the sites of positive MVI were documented. All disagreements were resolved by consensus.

MRI examination

All patients underwent 3.0 T MRI with six sequences of Gd-EOB-DTPA enhancement and DWI (Discovery MR750, GE Healthcare, Waukesha, WI, United States; Prisma and MAGNETOM Verio, Siemens Healthcare, Erlangen, Germany), including T1WI, T2WI, DWI, and post-injection phases of EOB as AP, PVP, and HBP. Detailed descriptions of the imaging acquisition protocols are summarized in Supplementary Table 1. For advanced DWI image quality, respiratory triggering, propeller, and resolve technical proposals were adopted.

Conventional radiological features analysis

Conventional radiological features were carefully evaluated based on the Liver Imaging Reporting and Data System (LI-RADS v2018), which included the tumor size, AP hyperenhancement, blood products in mass, capsule, corona enhancement, delayed central enhancement, diffusion restriction, fat or iron in mass more than the adjacent liver, fat or iron sparing in a solid mass, mosaic appearance, hepatobiliary phase hypointensity, hepatobiliary phase isointensity, and nodule-in-nodule appearance. The following MRI features were selected in this study: (1) Tumor size; the maximum diameter was measured on HBP axial images; (2) non-smooth tumor margin, which was defined as nodular with extranodular growth or multinodular confluence; (3) incomplete capsule, the region where the tumor border with liver tissue has no or incomplete capsule on portal venous phase or delayed phase; and (4) peritumoral hypointensity on HBP, wedge-shaped hypointense located outside of the tumor margin on HBP. After independent evaluation by three senior radiologists, discussions were conducted to reach a consensus wherever discrepancies occurred.

RADIOMICS SIGNATURES AND REPRODUCIBILITY ANALYSIS

Segmentation of the volume of interests

The Digital Imaging and Communications in Medicine images were transferred to the Big Data Intelligent Analysis Cloud Platform (Huiying Medical Technology Co., Ltd., Beijing, China). Two experts in liver MRI (senior radiologists with 15 and 25 years of experience) reviewed all images, and a radiologist manually segmented all target lesions who were blinded to the clinical information, creating a segmented volume of interest (VOI). After completion of the VOIs by a junior radiologist, the VOIs were reviewed by a senior radiologist for validation. To minimize the intensity variations caused by different scanning equipment and scanning parameters, these MR images were normalized by the standard deviation ($\mu - 3\sigma$, $\mu + 3\sigma$) before feature extraction, and all delineated VOIs were automatically analyzed (Figure 2).

As two radiologists measured the radiomics features to assess reproducibility, we calculated the intraclass correlation coefficient (ICC). When the ICC was > 0.80 , consistency was considered excellent.

Features extraction

We extracted 1409 quantitative imaging features from VOIs using the cloud platform big data intelligent analysis (<http://radcloud.cn/>). The features were categorized into four groups. The first-order statistical features were considered as group 1 (including a total of 18 descriptors), which delineated the distribution of voxel intensities in the MR images through common and basic metrics. Group 2 included shape- and size-based features (containing 14 three-dimensional features) that reflected the shape and size of the lesion areas. Group 3 included features of two-order texture, gray-level co-occurrence, and gray-level run-length texture matrices that were used to calculate those features, and 75 texture features were extracted to quantify the heterogeneity of lesions. The higher-order filter features such as group 4, Laplacian, wavelet, logarithmic, and exponential filters were applied to medical images, and then the first-order statistics and texture features were extracted based on the filtered image (1302 filter features).

Features selection

The least absolute shrinkage and selection operator (LASSO) was used to decrease irrelevance and redundancy. We performed a 10-fold cross-validation to select the optimal feature subset in LASSO regression, which was based on binomial deviance minimization criteria from the training cohort with a

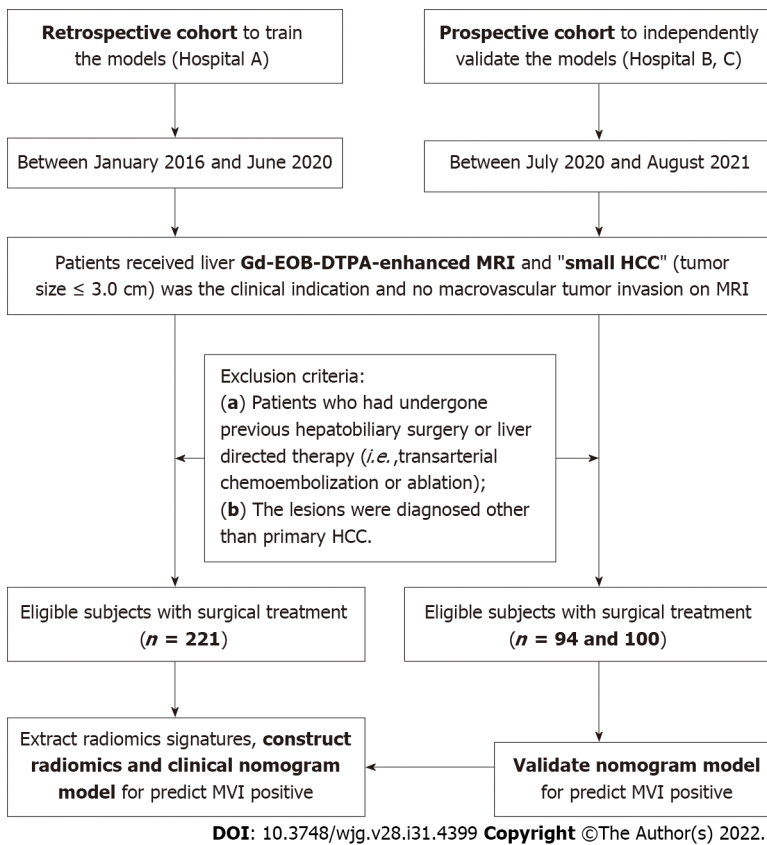


Figure 1 Flow diagram of the study cohort. A total of 415 participants were included in this multi-center study.

maximum iteration of 2000. A variance threshold of 0.8 was used for the selected eigenvalues of the variance.

Model development and validation

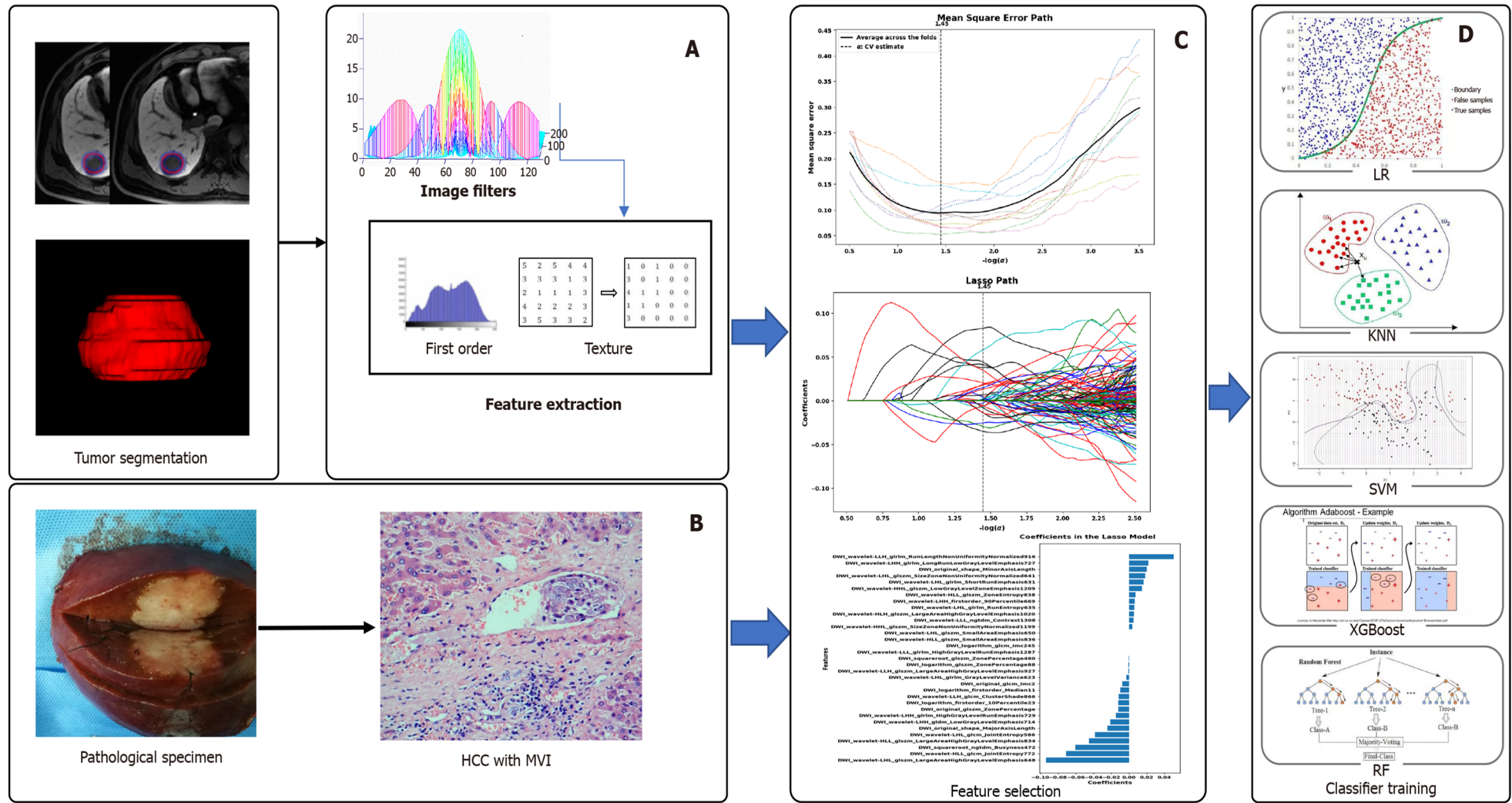
The retrospective data (Hospital A) were separated from the training and testing datasets using a random method with a ratio of 7:3, and external data (Hospitals B and C) as the independent validation sets. After feature qualification, based on the selected features, several machine learning classifiers can be used for classification analysis, creating models that can separate or predict MVI-positive data. In this study, radiomics-based LASSO models (machine learning) were constructed using T1WI, T2WI, DWI, AP, PVP, and HBP. We selected K-nearest neighbor (KNN), support vector machine (SVM), extreme gradient boosting (XGBoost), random forest (RF), logistic regression (LR), and decision tree (DT) as the machine learning classifiers, and the effectiveness of the model was improved using the validation method (Figure 2).

Confirmation of radiomics nomogram

R package (version 3.0, <http://www.r-project.org/>) was used to analyze the radiomics nomogram. Multivariate logistic regression analysis was performed to develop a model for predicting MVI, and all variables associated with MVI at a significant level were candidates for stepwise multivariate analysis. A nomogram was constructed based on the results of the multivariate logistic regression analysis. The receiver operating characteristic (ROC) curve was used to calculate the discrimination performance of the established models, and the values of the area under the curve (AUC) were compared using the Delong non-parametric approach. The calibration of the radiomics model was assessed using calibration curves. External data from the independent validation sets (hospitals B and C) were used to test the performance of the radiomics model. Finally, we constructed decision curves by calculating the net benefits for a range of threshold probabilities.

Statistical analyses

MedCalc 16.2.1 (Ostend, Belgium) and SPSS (version 22.0; Armonk, NY, United States) were used for the statistical analyses. The Kolmogorov-Smirnov method was used to identify the normal distribution of continuous variables. The differences in categorical and continuous variables were compared using the χ^2 test, Fisher's exact test, two-sample *t*-test, or Mann-Whitney *U* test, respectively. ROC analyses were performed to evaluate the predictive performance of MVI for sHCC. The Youden index was used for determining the cut-off values. Then, the AUC, sensitivity, and specificity were calculated, and a *Z*



DOI: 10.3748/wjg.v28.i31.4399 Copyright ©The Author(s) 2022.

Figure 2 Flow diagram for the radiomics of machine learning. A: Construct radiomics models, the volume of interest was delineated by experienced radiologists and three-dimensional images were formed, extracting quantitative features by software; B: Pathologic examination, firstly obtaining specimens of small hepatocellular carcinoma tissue, and then taking pathologic diagnosis for microvascular invasion; C: Data cleaning and dimensions reduction; D: Establishing the model for predicting microvascular invasion by machine learning. LR: Logistic regression; KNN: K-Nearest neighbor; SVM: Support vector machine; RF: Random forest.

test was used to compare the differences between the AUCs. Statistical significance was set at $P < 0.05$.

RESULTS

Patients and serological examinations

A total of 415 patients with qualified sHCC were enrolled in the final study (Figure 1). In hospitals A, B, and C, the mean participant age was 51.2 ± 10.9 (range 29-78) years, 53.04 ± 10.59 (range 28-77) years, and 54.01 ± 10.82 (range 28-85) years, respectively. Histological examination confirmed MVI in 64 (28.9%), 22 (23.4%), and 16 (16.0%) patients. The number of patients with hepatitis B, C and alcoholic hepatitis were 162 (73.3%), 21 (9.5%), 29 (13.1%); 71 (75.6%), 10 (10.6%), 8 (8.5%); and 82 (82.0%), 6 (6.0%), 2 (2.0%), respectively. The numbers of patients with cirrhosis were 173 (78.3%), 69 (73.4%), and 70 (70%), respectively. The median serum AFP levels were 26.10 (range 0.98-25451.00) ng/mL, 9.34 (range 1.09-6740.42) ng/mL, and 31.070 (range 0.713-4587.000) ng/mL, respectively. The median serum total bilirubin levels were 12.5 (range 2.9-64.6) $\mu\text{mol/L}$, 17.4 (range 3.6-446.9) $\mu\text{mol/L}$ and 13.2 (range 4.4-47.2) $\mu\text{mol/L}$, respectively. The median direct bilirubin levels were 3.9 (range 1.0-17.0) $\mu\text{mol/L}$, 4.5 (range 1.0-218.9) $\mu\text{mol/L}$ and 5.50 (range 1.50-26.84) $\mu\text{mol/L}$, respectively. The MELD scores were 13.9 ± 4.8 (range 7.0-26.9), 13.8 ± 5.8 (range 6.0-35.5) and 11.8 ± 4.5 (range 5.2-25.6). The number of Child-Pugh classes A, B, and C were 205 (93.2%), 13 (5.9%), 2 (0.9%), 81 (86.2%), 12 (12.8%), 1 (1.1%), 86 (86.0%), 13 (13.0%), and 1 (1.0%), respectively. There were 32 (14.5%), 142 (64.3%), 47 (21.2%); 12 (12.8%), 68 (72.3%), 14 (14.9%) and 8 (8.0%), 71 (71.0%), 21 (21.0%) cases that were histological grades I, II, and III, respectively (Table 1).

Conventional radiological features

In the group comparison of MVI-positive and negative, the AFP and tumor size were 33.91 (range 1.4-25451.0) and 22.52 (range 0.98-18929.00) (ng/mL) ($P = 0.026$), 2.34 ± 0.56 and 1.92 ± 0.67 (cm) ($P = 0.036$) in hospital A; 38.97 (range 1.90-6740.40) and 5.43 (range 1.10-2018.79) (ng/mL) ($P = 0.01$), 2.43 ± 0.57 and 2.11 ± 0.66 (cm) ($P = 0.047$) in hospital B; 109.72 (range 0.80-2278.00) and 24.41 (range 0.71-4587.00) (ng/mL) ($P = 0.032$), 2.47 ± 0.43 and 2.21 ± 0.64 (cm) ($P = 0.054$) in hospital C. In the MVI-positive group, the proportion of patients with non-smooth tumor margin, incomplete capsule, and peritumoral hypointensity was 39.7% (27/68) ($P = 0.019$), 40.3% (25/62) ($P = 0.02$), and 51.5% (17/33) ($P = 0.002$) in hospital A; 52.9% (9/17) ($P = 0.003$), 59.5% (25/42) ($P = 0.062$), and 35.7% (5/14) ($P = 0.304$) in hospital B; and 31.3% (10/32) ($P = 0.004$), 14.6% (6/41) ($P = 0.759$), and 63.6% (14/22) ($P = 0.002$) in hospital C (Table 2).

For discriminating MVI-positive, in hospital A, B and C the AUC of AFP was 0.597 [95% confidence interval (CI):0.528-0.662], 0.683 (95%CI:0.528-0.662) and 0.669 (95%CI:0.568-0.760), respectively; the AUC of tumor size was 0.675 (95%CI:0.609-0.736), 0.639 (95%CI:0.553-0.735) and 0.576 (95%CI:0.473-0.675), respectively; the AUC of non-smooth tumor margin was 0.580 (95%CI:0.512-0.646), 0.649 (95%CI:0.544-0.745) and 0.682 (95%CI:0.581-0.771), respectively; the AUC of incomplete capsule was 0.577 (95%CI:0.509-0.643), 0.595 (95%CI:0.489-0.695) and 0.521 (95%CI:0.419-0.622), respectively; the AUC of peritumoral hypointensity on HBP was 0.582 (95%CI:0.514-0.648), 0.551 (95%CI:0.445-0.654) and 0.667 (95%CI:0.565-0.758), respectively (Table 3).

Radiomics signatures

There were 155 and 66 patients with sHCC in the training and test datasets, respectively. The proportions of MVI-positive patients were 27.1% and 29%, respectively. There were no significant differences in patient characteristics between the training and testing cohorts ($P > 0.05$). Among the 1409 radiomics features in each T1WI, T2WI, DWI, AP, PVP, and HBP model, 443, 483, 467, 554, 462, and 453 features were selected based on a variance threshold of over 0.80. After LASSO analysis, five, 22, 33, four, eight, and 30 features were selected for T1WI, T2WI, DWI, AP, PVP, and HBP, respectively.

Robustness analysis results

We found that 70.5% (993/1409) of the features extracted from T1WI images had excellent consistency (ICC > 0.8), and all five features selected for modeling had excellent consistency (ICC median, 0.969; minimum, 0.877; maximum, 1.000). The features of 51.9% (731/1409) extracted from T2WI images had excellent consistency (ICC > 0.8), and most of the 22 features selected for modeling had good consistency (ICC median, 0.701; minimum, 0.41; maximum, 0.94). The features of 60.04% (846/1409) extracted from DWI images had excellent consistency (ICC > 0.8), and most of the 33 features selected for modeling had excellent consistency (ICC median, 0.869; minimum, 0.41; maximum, 0.98). The features of 67.8% (956/1409) extracted from AP images had excellent consistency (ICC > 0.8), and the ICC of the four features selected for modeling were 0.902, 0.884, 0.734, and 0.891. The features of 62.1% (875/1409) extracted from PVP images had excellent consistency (ICC > 0.8), and most of the eight features selected for modeling had excellent consistency (ICC median = 0.844, minimum = 0.500, maximum = 1.000). The features of 82.5% (1163/1409) extracted from HBP images had excellent consistency (ICC > 0.8), and most of the 30 features selected for modeling had excellent consistency (ICC

Table 1 Demographics, alpha fetal protein, bilirubin, tumor characteristics, and microvascular infiltration of the patients with small hepatocellular carcinoma in data sets of three hospitals

| Characteristics | Hospital A (n = 221) | Hospital B (n = 94) | Hospital C (n = 100) |
|-------------------------|--|--|--|
| Age (yr) | mean ± SD: 51.2 ± 10.9 (range 29-78) | mean ± SD: 53.04 ± 10.59 (range 28-77) | mean ± SD: 54.01 ± 10.82 (range 28-85) |
| Male/female | 189 (85.5%)/32 (14.5%) | 84 (89.4%)/10 (10.6%) | 85 (85.5%)/15 (15.0%) |
| Causes of liver disease | | | |
| Hepatitis B | 162 (73.3%) | 71 (75.6%) | 82 (82.0%) |
| Hepatitis C | 21 (9.5%) | 10 (10.6%) | 6 (6.0%) |
| Alcoholic hepatitis | 29 (13.1%) | 8 (8.5%) | 2 (2.0%) |
| Others | 9 (4.1%) | 5 (5.3%) | 10 (10.0%) |
| Cirrhosis | | | |
| Present | 173 (78.3%) | 69 (73.4%) | 70 (70%) |
| Absent | 48 (21.7%) | 25 (26.6%) | 30 (30%) |
| AFP (ng/mL) | Median: 26.10 (range 0.98-25451.00) | Median: 9.34 (range 1.09-6740.42) | Median: 31.070 (range 0.713- 4587.000) |
| TbIL (μmol/L) | Median: 12.5 (range 2.9-64.6) | Median: 17.4 (range 3.6-446.9) | Median: 13.2 (range 4.4-47.2) |
| DBiL (μmol/L) | Median: 3.9 (range 1.0-17.0) | Median: 4.5 (range 1.0-218.9) | Median: 5.50 (range 1.50-26.84) |
| MELD scores | mean ± SD: 13.9 ± 4.8 (range 7.0-26.9) | mean ± SD: 13.8 ± 5.8 (range 6.0-35.5) | mean ± SD: 11.8 ± 4.5 (range 5.2-25.6) |
| Child-Pugh classes | | | |
| A | 205 (93.2%) | 81 (86.2%) | 86 (86.0%) |
| B | 13 (5.9%) | 12 (12.8%) | 13 (13.0%) |
| C | 2 (0.9%) | 1 (1.1%) | 1 (1.0%) |
| Edmondson-steiner grade | | | |
| Grade I | 32 (14.5%) | 12 (12.8%) | 8 (8.0%) |
| Grade II | 142 (64.3%) | 68 (72.3%) | 71 (71.0%) |
| Grade III | 47 (21.2%) | 14 (14.9%) | 21 (21.0%) |
| Tumor size (cm) | mean ± SD: 2.04 ± 0.67 (range 0.60-3.00) | mean ± SD: 2.17 ± 0.42 (range 0.80-3.00) | mean ± SD: 2.20 ± 0.41 (range 0.90-3.00) |
| MVI | | | |
| Positive | 64 (28.9%) | 22 (23.4%) | 16 (16.0%) |
| Negative | 157 (71.1%) | 72 (76.6%) | 84 (84.0%) |

TbIL: Total bilirubin; DBiL: Direct bilirubin; MELD: Model for end-stage liver disease; AFP: Alpha-fetoprotein; MVI: Microvascular infiltration.

median, 0.917; minimum, 0.690; maximum, 1.000).

Predictive performance of the machine learning classifiers

The machine learning classifiers used in this study were KNN, LR, MLP, RF, SVM, and DT. In general, all classifiers achieved satisfactory performance, with LR being the best machine learning method. To predict MVI, T1WI, T2WI, DWI, AP, PVP, and HBP radiomics models were constructed and validated. In the testing set, the AUCs were 0.776 (95% CI: 0.611-0.895), 0.813 (95% CI: 0.651-0.922), 0.971 (95% CI: 0.858-0.999), 0.788 (95% CI: 0.642-0.894), 0.790 (95% CI: 0.630-0.904) and 0.979 (95% CI: 0.911-1.000). In validation hospital B, the AUCs were 0.834 (95% CI: 0.742-0.904), 0.825 (95% CI: 0.732-0.896), 0.816 (95% CI: 0.678-0.876), 0.810 (95% CI: 0.715-0.884), 0.847 (95% CI: 0.758-0.913) and 0.970 (95% CI: 0.912-0.994). In validation hospital C, the AUCs were 0.766 (95% CI: 0.672-0.844), 0.761 (95% CI: 0.669-0.839), 0.801 (95% CI: 0.710-0.871), 0.824 (95% CI: 0.737-0.892), 0.833 (95% CI: 0.748-0.898) and 0.803 (95% CI: 0.680-0.834) (Figure 3, Table 4).

Development and validation of MVI predicting nomogram

The C-indexes of the radiomics and clinic combined nomogram with the model of T1WI, T2WI, DWI, AP, PVP and HBP were 0.771 (95% CI: 0.695-0.836), 0.895 (95% CI: 0.834-0.940), 0.990 (95% CI: 0.957-0.999), 0.774 (95% CI: 0.706-0.833), 0.746 (95% CI: 0.668-0.814) and 0.990 (95% CI: 0.944-0.993) in the training set,

Table 2 Age, gender, alpha-fetoprotein and radiologic features of patients with small hepatocellular carcinoma and relationship with microvascular infiltration

| | Hospital A (n = 221) | | | Hospital B (n = 94) | | | Hospital C (n = 100) | | |
|---------------------------|-----------------------------|-----------------------|---------|----------------------------|---------------------------|---------|-----------------------------|----------------------------|---------|
| | Positive | Negative | P value | Positive | Negative | P value | Positive | Negative | P value |
| Age (yr) | 50.9 ± 10.7 | 51.3 ± 10.9 | 0.840 | 51.7 ± 12.3 | 53.1 ± 10.1 | 0.597 | 53.5 ± 9.1 | 53.7 ± 11.0 | 0.958 |
| Gender | | | 0.593 | | | 0.443 | | | 0.259 |
| Female | 8 | 24 | | 1 | 9 | | 1 | 14 | |
| Male | 56 | 133 | | 21 | 63 | | 15 | 70 | |
| AFP (ng/mL) | 33.91 (range 1.40-25451.00) | 22.52 (range 1-18929) | 0.026 | 38.97 (range 1.90-6740.40) | 5.43 (range 1.10-2018.79) | 0.010 | 109.72 (range 0.80-2278.00) | 24.41 (range 0.71-4587.00) | 0.032 |
| Size (cm) | 2.34 ± 0.56 | 1.92 ± 0.67 | 0.036 | 2.43 ± 0.57 | 2.11 ± 0.66 | 0.047 | 2.47 ± 0.43 | 2.21 ± 0.64 | 0.054 |
| Nonsmooth tumor margin | | | 0.019 | | | 0.003 | | | 0.004 |
| Absent | 37 | 116 | | 13 | 64 | | 6 | 62 | |
| Present | 27 | 41 | | 9 | 8 | | 10 | 22 | |
| Capsule | | | 0.020 | | | 0.062 | | | 0.756 |
| Absent | 39 | 120 | | 21 | 55 | | 10 | 49 | |
| Present | 25 | 37 | | 25 | 17 | | 6 | 35 | |
| Peritumoral hypointensity | | | 0.002 | | | 0.304 | | | 0.007 |
| Absent | 47 | 141 | | 17 | 63 | | 70 | 8 | |
| Present | 17 | 16 | | 5 | 9 | | 14 | 8 | |

Size: Large tumor size; AFP: Alpha-fetoprotein; MVI: Microvascular infiltration.

respectively; 0.846 (95%CI: 0.594-0.883), 0.917 (95%CI: 0.640-0.915), 0.970 (95%CI: 0.843-0.997), 0.794 (95%CI: 0.615-0.876), 0.831 (95%CI: 0.650-0.916) and 0.971 (95%CI: 0.892-0.999) in the testing set, respectively; 0.895 (95%CI: 0.775-0.925), 0.886 (95%CI: 0.746-0.906), 0.843 (95%CI: 0.685-0.881), 0.886 (95%CI: 0.695-0.899), 0.918 (95%CI: 0.791-0.934) and 0.912 (95%CI: 0.918-0.996) in validation hospital B, respectively; 0.830 (95%CI: 0.667-0.850), 0.808 (95%CI: 0.654-0.867), 0.869 (95%CI: 0.694-0.899), 0.874 (95%CI: 0.674-0.884), 0.870 (95%CI: 0.732-0.887) and 0.808 (95%CI: 0.635-0.892) in validation hospital C, respectively (Figure 4, Table 5).

Decision curve analysis showed adequate performance for radiomics nomogram models for predicting MVI in sHCC. The proposed radiomics model to predict MVI showed a greater advantage than the “clinikoradiological” scheme ($P < 0.05$). There was no significant difference in predictive efficacy between the combination nomogram model and the single radiomics model ($P > 0.05$) (Figure 5).

DISCUSSION

In this multi-center study, we analyzed the clinical and imaging data of 415 patients with sHCC who underwent DWI, Gd-EOB-DTPA-enhanced MRI, and hepatectomy. We used a machine learning approach to construct radiomics signatures and nomogram models for preoperative prediction of MVI and then independently validated the machine learning and nomogram models. Our data showed that clinical and common MRI radiological features, including AFP, tumor size, non-smooth tumor margin, incomplete capsule, and HBP peritumoral hypointensity, have limited diagnostic value for MVI of sHCC. The LR classifier was the best machine learning method, and the radiomics scores of HBP and DWI had great diagnostic efficiency for predicting MVI of sHCC. The nomogram model of combined radiomics scores, APF, and common MRI features exhibited good calibration and discrimination in the training, testing, and independent external validation cohorts.

Gd-EOB-DTPA with a pendant ethoxybenzyl group covalently attached to gadopentetate dimeglumine is a hepatocyte-specific MRI contrast agent that can be taken up by hepatocytes *via* the organic anion transporting polypeptides[30]. Gd-EOB-DTPA, which has dual extracellular and hepatobiliary

Table 3 Diagnostic performance of alpha-fetoprotein and radiologic features for assessing microvascular infiltration of small hepatocellular carcinoma by receiver operating characteristic curve analysis

| | AFP | Tumor size | Nonsmooth tumor margin | Incomplete capsule | Peritumoral hypointensity |
|----------------|-------------|-------------|------------------------|--------------------|---------------------------|
| Hospital A | | | | | |
| AUC | 0.597 | 0.675 | 0.580 | 0.577 | 0.582 |
| 95%CI | 0.528-0.662 | 0.609-0.736 | 0.512-0.646 | 0.509-0.643 | 0.514-0.648 |
| <i>P</i> value | 0.024 | < 0.001 | 0.024 | 0.027 | 0.007 |
| Sensitivity | 34.92 | 70.31 | 42.19 | 39.06 | 26.56 |
| Specificity | 81.82 | 61.15 | 73.89 | 76.43 | 89.81 |
| Hospital B | | | | | |
| AUC | 0.683 | 0.639 | 0.649 | 0.595 | 0.551 |
| 95%CI | 0.577-0.777 | 0.553-0.735 | 0.544-0.745 | 0.489-0.695 | 0.445-0.654 |
| <i>P</i> value | 0.006 | 0.035 | 0.008 | 0.005 | 0.304 |
| Sensitivity | 63.64 | 81.82 | 71.43 | 95.45 | 22.73 |
| Specificity | 72.06 | 44.44 | 88.89 | 23.61 | 87.50 |
| Hospital C | | | | | |
| AUC | 0.669 | 0.576 | 0.682 | 0.521 | 0.667 |
| 95%CI | 0.568-0.760 | 0.473-0.675 | 0.581-0.771 | 0.419-0.622 | 0.565-0.758 |
| <i>P</i> value | 0.016 | 0.213 | 0.007 | 0.759 | 0.014 |
| Sensitivity | 87.50 | 68.75 | 62.50 | 62.50 | 50.00 |
| Specificity | 52.38 | 54.76 | 73.81 | 41.67 | 83.33 |

DeLong test for comparison of receiver operating characteristic curve. AFP: Alpha-fetoprotein; AUC: Area under the curve; 95%CI: 95% confidence interval.

properties that provide structural and functional information on liver lesions, can also provide information on nonspecific gadolinium chelates during dynamic enhancement[31,32]. Granito *et al*[33] reported that Gd-EOB-DTPA-enhanced MRI may improve the sensitivity of noninvasive diagnosis of small HCC nodules in patients with cirrhosis, and the double hypointensity in the portal/venous and HBP can be regarded as an MRI pattern, which is highly suggestive of hypovascular hepatocellular carcinoma. This previous study revealed that large tumor size, incomplete capsule, non-smooth tumor margin, peritumoral enhancement on AP, and peritumoral hypointensity on HBP could achieve predictive AUCs of up to 0.85 for MVI of HCC[34]. However, for small HCC (large tumor size ≤ 3 cm), the common MRI radiologic features are smooth tumor margin, complete capsule (or no capsule), and no peritumoral hypointensity in HBP. In this study, the results from three hospitals showed that these conventional MRI radiologic features had limited value in evaluating MVI for sHCC.

Based on these characteristics, we established a Gd-EOB-DTPA MRI radiomics model using machine learning to construct and validate radiomics models for predicting MVI of sHCC. Machine learning has demonstrated capabilities to learn and even master complex tasks, making it useful for computer-aided diagnosis and decision support systems[21]. Radiomics refers to a technique of high-throughput extraction of quantitative imaging features or textures to decode histology and create a high-dimensional dataset[35]. However, it was thought that the parameters of the MRI scanner would not have an obvious influence on the results of radiomics analysis after the images were standardized when a previous multi-center study[36] did not demand the same MRI scanners and parameters. However, to minimize the possible influence of other factors, a unified MRI scanner and image standardization process were used in our study. Furthermore, whole-tumor volume analysis was used to decrease sampling bias.

Although previous studies have verified that the radiomics features of CT imaging could predict MVI status in patients with HCC preoperatively, it has high diagnostic efficiency, and the AUC can reach approximately 0.85[27,37]. In addition, Feng *et al*[38] evaluated Gd-EOB-DTPA-enhanced MRI quantitative features of peri- and intratumoral regions, providing a radiomics model for MVI prediction in patients with HCC. In the validation cohort, the AUC, sensitivity, and specificity were 0.83%, 90.00%, and 75.00%, respectively. However, none of these studies predicted the MVI for sHCC or provided a clinical nomogram. In this study, we extracted radiomics signatures from images of Gd-EOB-DTPA-

Table 4 Receiver operator characteristic curve analysis of radiomics scores with different sequences of magnetic resonance imaging for predict microvascular infiltration of small hepatocellular carcinoma

| | T1WI | T2WI | DWI | AP | PVP | HBP |
|-----------------------|-------------|-------------|-------------|-------------|-------------|-------------|
| Training set | | | | | | |
| AUC | 0.740 | 0.878 | 0.991 | 0.763 | 0.739 | 0.976 |
| 95%CI | 0.661-0.808 | 0.814-0.926 | 0.958-0.999 | 0.695-0.823 | 0.661-0.807 | 0.940-0.991 |
| <i>P</i> value | < 0.001 | < 0.001 | < 0.001 | < 0.001 | < 0.001 | < 0.001 |
| Sensitivity | 77.08 | 82.98 | 95.74 | 71.43 | 56.25 | 89.83 |
| Specificity | 68.00 | 82.00 | 96.04 | 79.37 | 78.22 | 99.27 |
| Testing set | | | | | | |
| AUC | 0.776 | 0.813 | 0.971 | 0.788 | 0.790 | 0.979 |
| 95%CI | 0.611-0.895 | 0.651-0.922 | 0.858-0.999 | 0.642-0.894 | 0.630-0.904 | 0.911-1.000 |
| <i>P</i> value | 0.0004 | < 0.001 | < 0.001 | 0.0014 | 0.0001 | < 0.001 |
| Sensitivity | 91.67 | 58.33 | 100.00 | 64.29 | 84.62 | 100.00 |
| Specificity | 57.69 | 92.00 | 84.62 | 93.75 | 73.08 | 91.43 |
| Validation Hospital B | | | | | | |
| AUC | 0.834 | 0.825 | 0.816 | 0.810 | 0.847 | 0.970 |
| 95%CI | 0.742-0.904 | 0.732-0.896 | 0.678-0.876 | 0.715-0.884 | 0.758-0.913 | 0.912-0.994 |
| <i>P</i> value | < 0.001 | < 0.001 | 0.0002 | < 0.001 | < 0.001 | < 0.001 |
| Sensitivity | 63.64 | 95.45 | 71.43 | 57.14 | 54.55 | 95.45 |
| Specificity | 94.29 | 57.75 | 88.89 | 88.89 | 98.61 | 98.57 |
| Validation Hospital C | | | | | | |
| AUC | 0.766 | 0.761 | 0.801 | 0.824 | 0.833 | 0.803 |
| 95%CI | 0.672-0.844 | 0.669-0.839 | 0.710-0.871 | 0.737-0.892 | 0.748-0.898 | 0.680-0.834 |
| <i>P</i> value | 0.0001 | 0.0003 | < 0.001 | < 0.001 | < 0.001 | 0.007 |
| Sensitivity | 80.00 | 60.00 | 90.00 | 86.67 | 85.71 | 83.33 |
| Specificity | 70.45 | 89.01 | 68.89 | 68.54 | 72.83 | 77.67 |

T1WI: T1 weighted imaging; T2WI: T2 weighted imaging; DWI: Diffusion weighted imaging; AP: Arterial phase; PVP: Portal vein phase; HBP: Hepatobiliary phase; AUC: Area under the curve; 95%CI: 95% confidence interval.

enhanced MRI and then built the model using T1WI, T2WI, AP, PVP, and HBP. The results illustrated that radiomics has the best modeling in HBP and DWI when the LR and classifier of machine learning are utilized, producing great diagnostic efficiency for predicting MVI. Furthermore, the independent external validation results confirmed this efficiency. This may be because the post-Gd-EOB-DTPA contrast enhancement images provide structural and functional information on HBP lesions. The LR algorithm is used to establish a cost function for a classification or regression problem and then solve the optimal model iteratively through the optimization method.

Our results also demonstrate that the radiomics characteristics of DWI images can accurately predict the MVI of sHCC. DWI is an MRI technology that can reflect the motion of water molecules *in vivo* and can be used to assess tumor cellularity[39]. HCC with MVI is more likely to have higher cellularity and poor differentiation than HCC without MVI[40]. Okamura *et al*[41] suggested that the apparent diffusion coefficient (ADC) value is a valuable predictor of poor differentiation and MVI and is significantly related to tumor recurrence. Kim *et al*[42] illustrated that the tumor-to-liver ADC ratio was a significant independent parameter for the MVI of sHCC and the degree of lymphocyte infiltration. Our research further extracted the radiomics characteristics of the tumor, which were based on DWI images that confirmed that the quantitative characteristics of the radiomics had good performance for predicting the MVI of sHCC.

A nomogram was built in our study, which converted each regression coefficient proportionally in multivariate logistic regression to a 0- to 100-point scale. The effect of features with the absolute value of the highest β coefficient was assigned 100 points. The total points of the independent variables were

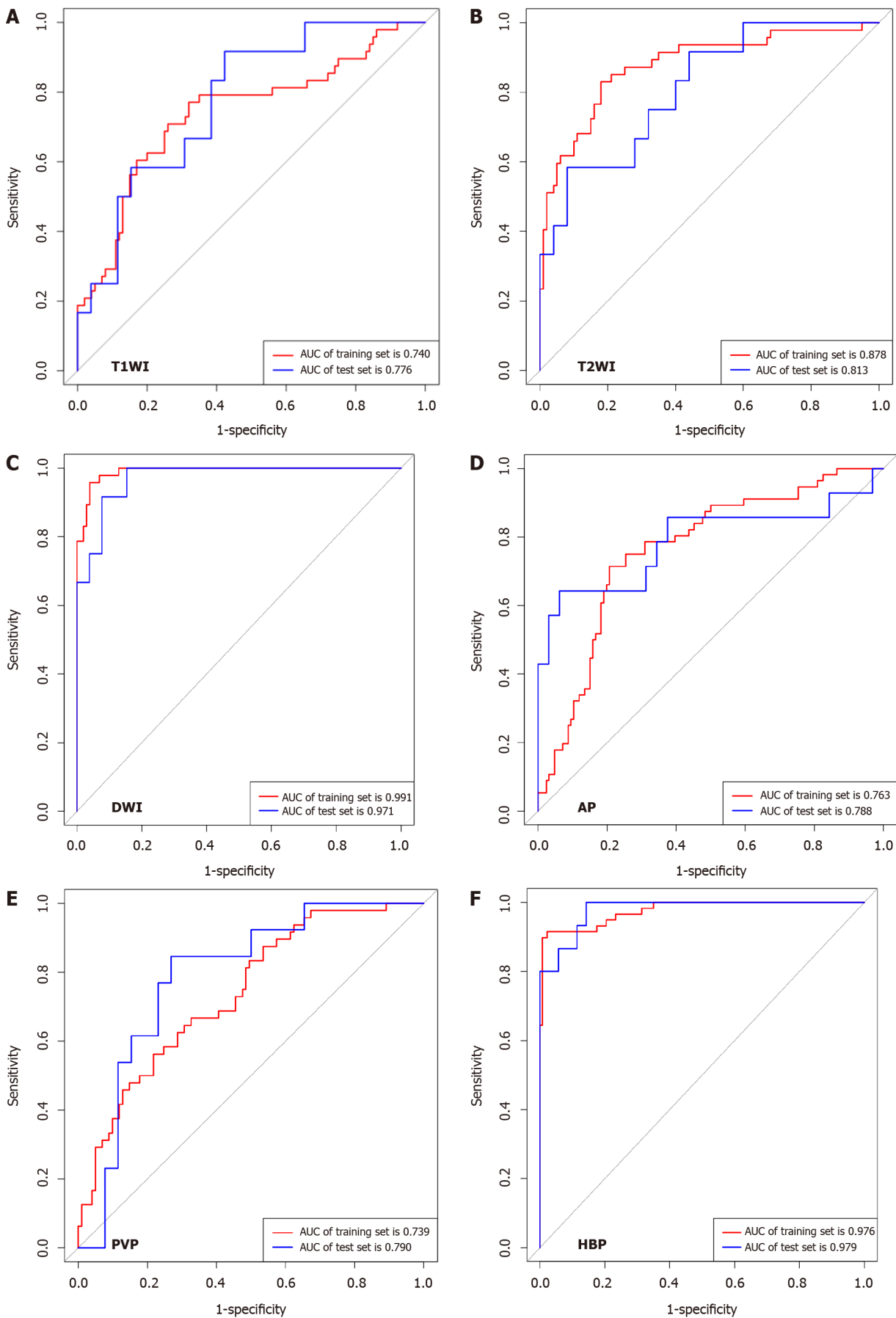
Table 5 Predictive performance of the nomogram prediction model for estimating the risk of microvascular infiltration presence in patients with small hepatocellular carcinoma

| | Training set | Testing set | Validation Hospital B | Validation Hospital C |
|----------------|--------------|-------------|-----------------------|-----------------------|
| T1WI | | | | |
| C-index | 0.771 | 0.846 | 0.895 | 0.830 |
| 95%CI | 0.695-0.836 | 0.594-0.883 | 0.775-0.925 | 0.667-0.850 |
| <i>P</i> value | < 0.001 | 0.0014 | < 0.001 | 0.0001 |
| T2WI | | | | |
| C-index | 0.895 | 0.917 | 0.886 | 0.808 |
| 95%CI | 0.834-0.940 | 0.640-0.915 | 0.746-0.906 | 0.654-0.867 |
| <i>P</i> value | < 0.001 | 0.0001 | < 0.001 | 0.0015 |
| DWI | | | | |
| C-index | 0.990 | 0.970 | 0.843 | 0.869 |
| 95%CI | 0.957-0.999 | 0.843-0.997 | 0.685-0.881 | 0.694-0.899 |
| <i>P</i> value | < 0.001 | < 0.001 | 0.0001 | < 0.001 |
| AP | | | | |
| C-index | 0.774 | 0.794 | 0.886 | 0.874 |
| 95%CI | 0.706-0.833 | 0.615-0.876 | 0.695-0.899 | 0.674-0.884 |
| <i>P</i> value | < 0.001 | 0.0025 | < 0.001 | < 0.001 |
| PVP | | | | |
| C-index | 0.746 | 0.831 | 0.918 | 0.870 |
| 95%CI | 0.668-0.814 | 0.650-0.916 | 0.791-0.934 | 0.732-0.887 |
| <i>P</i> value | < 0.001 | < 0.001 | < 0.001 | < 0.001 |
| HBP | | | | |
| C-index | 0.990 | 0.971 | 0.912 | 0.808 |
| 95%CI | 0.944-0.993 | 0.892-0.999 | 0.918-0.996 | 0.635-0.892 |
| <i>P</i> value | < 0.001 | < 0.001 | < 0.001 | 0.0081 |

T1WI: T1 weighted imaging; T2WI: T2 weighted imaging; DWI: Diffusion weighted imaging; AP: Arterial phase; PVP: Portal vein phase; HBP: Hepatobiliary phase; 95%CI, 95% confidence interval; C-index: Concordance index.

converted to the predicted probabilities. The concordance index (C-index) was used to predict the performance of the nomogram and calibration with 1000 bootstrap samples to decrease the overfitting bias[43]. Our study incorporated six factors: radiomics signatures, APF, tumor size, non-smooth tumor margin, incomplete capsule, and peritumoral hypointensity. Radiomics combined with the clinico-radiological factors nomogram model achieved good concordance indices in predicting MVI in the training and validation cohorts. In particular, the nomogram with HBP and DWI radiomics model showed excellent predictive efficiency in the two external validation datasets, and decision curve analysis further confirmed the clinical usefulness of the nomogram.

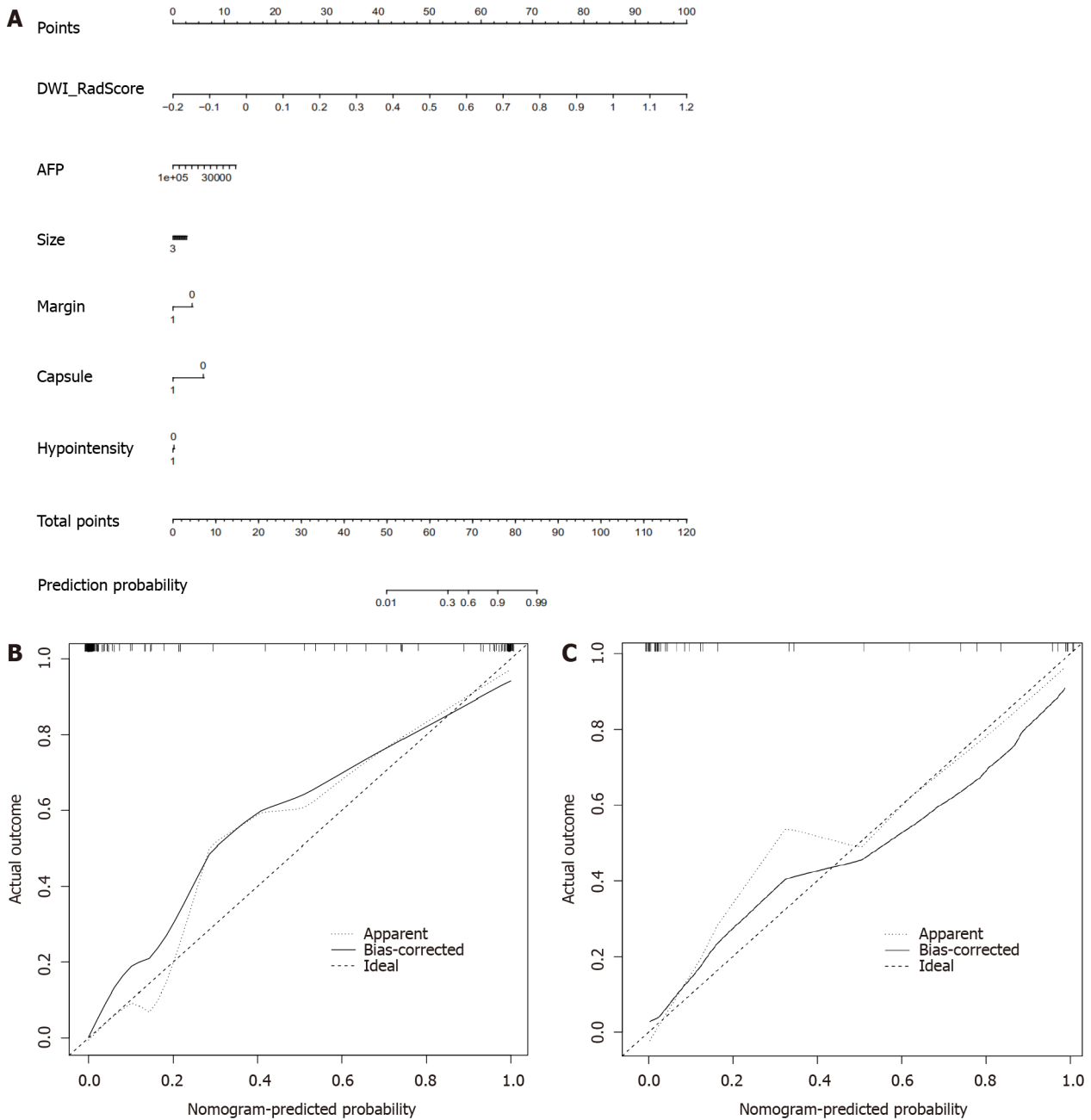
Nonetheless, this study had several limitations. First, the included patient population in this study had an inevitable bias in the inter-center distribution, although the application of radiomics and clinical nomogram was ensured by the multi-center nature of this study. To investigate the impact factors of bias on the baseline, we analyzed the age, AFP levels, liver function, and tumor size. Further larger-scale studies with more balanced subjects are needed to validate our results. Second, given the difficulty of collecting scalable medical imaging data for small HCC, many patients with small HCC who underwent transarterial chemoembolization or ablation could not be enrolled in the model of radiomics signatures and clinical nomogram to predict MVI. Given larger medical imaging datasets, deep networks are expected to improve prediction accuracy. Third, due to the lack of prognostic analysis in this study, we analyzed the different prognoses of sHCC patients with positive and negative MVI, which were predicted using a radiomics nomogram.



DOI: 10.3748/wjg.v28.i31.4399 Copyright ©The Author(s) 2022.

Figure 3 Receiver operating characteristic curve of different radiomics models for diagnosis microvascular invasion in small hepato-

cellular carcinoma (testing set). A: T1 weighted imaging [area under curve (AUC) was 0.776; 95% confidence interval (CI): 0.611-0.895]; B: T2 weighted imaging [AUC, 0.813; 95% confidence interval (CI): 0.651-0.922]; C: Diffusion weighted imaging (AUC, 0.971; 95%CI: 0.858-0.999); D: Arterial phase (AUC, 0.788; 95%CI: 0.642-0.894); E: Portal vein phase (AUC, 0.790; 95%CI: 0.630-0.904); F: Hepatobiliary phase (AUC, 0.990; 95%CI: 0.911-1.000). T1W1: T1 weighted imaging; T2W2: T2 weighted imaging; AUC: Area under curve; DWI: Diffusion weighted imaging; AP: Arterial phase; PVP: Portal vein phase; HBP: Hepatobiliary phase.

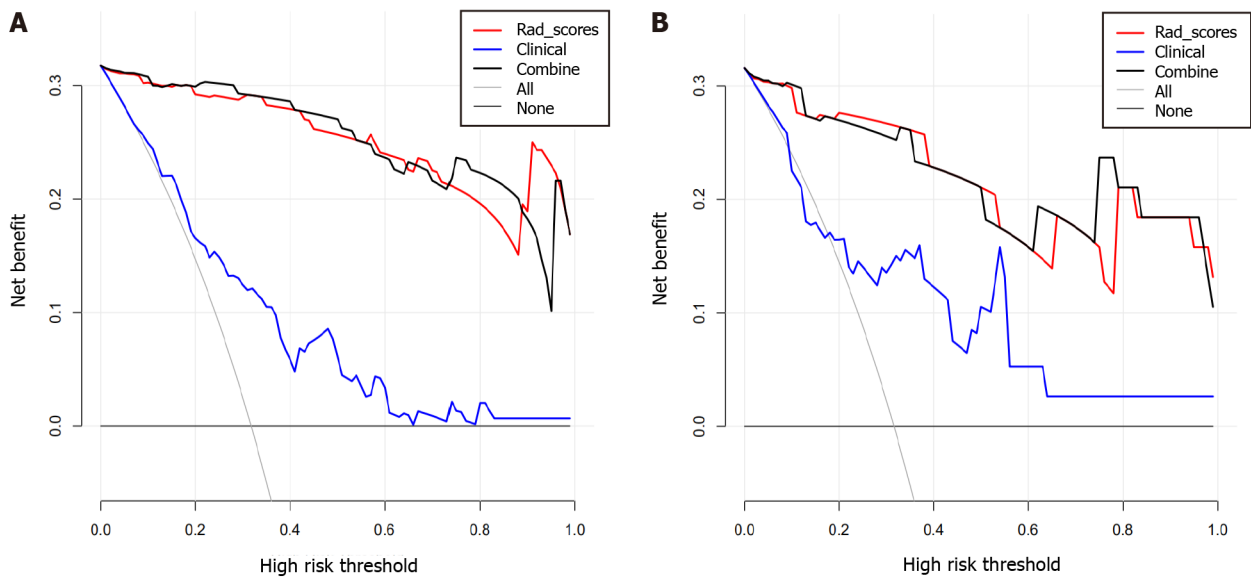


DOI: 10.3748/wjg.v28.i31.4399 Copyright ©The Author(s) 2022.

Figure 4 Nomogram of diffusion weighted imaging radiomics model to predict microvascular invasion in patients with small hepatocellular carcinoma. A: The nomogram was developed with radiomics signature and clinicoradiological factors. A vertical line was drawn according to the value of radiomics scores to determine the corresponding value of points. Similarly, the points of tumor markers were determined. The total points were the sum of the two points above. Finally, a vertical line was made according to the value of the total points to determine the probability of microvascular invasion (MVI); B: Validity of the predictive performance of the nomogram in estimating the risk of MVI presence in the training cohort; C: Validity of the predictive performance of the nomogram in estimating the risk of MVI presence in the validation cohort. AFP: Alpha-fetoprotein; DWI: Diffusion weighted imaging; Rad_score: Radiomics signatures score.

CONCLUSION

In conclusion, our study revealed that AFP and conventional Gd-EOB-DTPA-enhanced MRI features



DOI: 10.3748/wjg.v28.i31.4399 Copyright ©The Author(s) 2022.

Figure 5 Decision curve analysis. A and B: Decision curve analysis of the prediction model for training (A) and testing (B) cohort. Y-axis represents the net benefit, which is calculated by gaining true positives and deleting false positives. The X-axis is the probability threshold. The curve of the radiomics and combined nomogram over the clinical features that integrated AFP and radiological signatures showed the greatest benefit. AFP: Alpha-fetoprotein; Rad_score: Radiomics signatures score.

have poor diagnostic accuracies for MVI in sHCC. The radiomic signatures of HBP and DWI can further improve the ability to predict MVI. Furthermore, as a noninvasive preoperative prediction method, the radiomics nomogram showed favorable predictive accuracy for evaluating MVI in sHCC, which may help reassess the clinical therapeutic regimen for patients with sHCC.

ARTICLE HIGHLIGHTS

Research background

Microvascular invasion (MVI) of hepatocellular carcinoma (HCC) is an independent poor prognostic factor.

Research motivation

It is difficult to determine MVI of small hepatocellular carcinoma (HCC) (≤ 3.0 cm) by preoperative MRI conventional features.

Research objectives

To develop and validate radiomics scores and nomogram of gadolinium ethoxybenzyl diethylenetriamine pentaacetic acid (Gd-EOB-DTPA)-enhanced magnetic resonance imaging (MRI) for preoperative prediction of MVI in sHCC.

Research methods

Radiomics models of Gd-EOB-DTPA enhanced MRI and diffusion weighted images were constructed and validated by machine learning from data sets of three hospitals. A nomogram prediction model was developed using multivariable logistic regression analysis which included the radiomics scores, radiologic features, and alpha-fetoprotein (AFP) level.

Research results

AFP and MRI conventional features had poor diagnostic value for MVI of small HCC. The nomogram model (combined radiomics and clinic features) exhibited good calibration and discrimination in the testing and two external validation cohorts (in the two external validation cohorts, C-index was 0.912 and 0.808, respectively).

Research conclusions

As a noninvasive preoperative prediction method, the MRI radiomics nomogram shows favorable predictive accuracy for evaluate MVI in sHCC.

Research perspectives

This clinical prediction model may help in the selection of treatment options for small HCC.

ACKNOWLEDGEMENTS

The authors would like to thank Yingying Ezell for the language recheck and editing, Fuling Huang for his technical support, and Huiting Zhang (Siemens Healthineers, Wuhan, Hubei Province, China) for her constructive suggestions during the MRI scanning.

FOOTNOTES

Author contributions: Chen YD and Zhang L contributed equally to this work; Chen YD and Long LL was the guarantor and designed the study; Zhang L, Lin B, Jiang ZJ, Tang C, Dang YW, and Xia YW participated in the acquisition, analysis, interpretation of the data, and drafted the initial manuscript; Zhou ZP and Song B revised the article critically for important intellectual content.

Supported by the National Natural Science Foundation of China, No. 82060310; and Science and Technology Support Program of Sichuan Province, No. 2022YFS0071.

Institutional review board statement: The study was reviewed and approved by The First Affiliated Hospital of Guangxi Medical University Ethical Review Committee, No. 2019 KY-E-65.

Informed consent statement: All study participants, or their legal guardian, provided informed written consent prior to study enrollment.

Conflict-of-interest statement: There are no conflicts of interest to report.

Data sharing statement: The data that support the findings of this study are available in the Baidu Netdisk or our AI Scientific Research Platform (<https://mics.radcloud.cn/>). Further enquiries can be directed to the corresponding author.

STROBE statement: The authors have read the STROBE Statement – checklist of items, and the manuscript was prepared and revised according to the STROBE Statement – checklist of items.

Open-Access: This article is an open-access article that was selected by an in-house editor and fully peer-reviewed by external reviewers. It is distributed in accordance with the Creative Commons Attribution NonCommercial (CC BY-NC 4.0) license, which permits others to distribute, remix, adapt, build upon this work non-commercially, and license their derivative works on different terms, provided the original work is properly cited and the use is non-commercial. See: <https://creativecommons.org/licenses/by-nc/4.0/>

Country/Territory of origin: China

ORCID number: Yi-Di Chen 0000-0001-6293-4624; Ling Zhang 0000-0001-7270-3555; Yi-Wu Dang 0000-0002-7793-1239; Bin Song 0000-0002-7269-2101; Li-Ling Long 0000-0003-3369-8532.

S-Editor: Chen YL

L-Editor: Filipodia

P-Editor: Yuan YY

REFERENCES

- 1 **Ghouri YA**, Mian I, Rowe JH. Review of hepatocellular carcinoma: Epidemiology, etiology, and carcinogenesis. *J Carcinog* 2017; **16**: 1 [PMID: 28694740 DOI: 10.4103/jcar.JCar_9_16]
- 2 **Xu J**. Trends in Liver Cancer Mortality Among Adults Aged 25 and Over in the United States, 2000-2016. *NCHS Data Brief* 2018; 1-8 [PMID: 30044212]
- 3 **Omata M**, Cheng AL, Kokudo N, Kudo M, Lee JM, Jia J, Tateishi R, Han KH, Chawla YK, Shiina S, Jafri W, Payawal DA, Ohki T, Ogasawara S, Chen PJ, Lesmana CRA, Lesmana LA, Gani RA, Obi S, Dokmeci AK, Sarin SK. Asia-Pacific clinical practice guidelines on the management of hepatocellular carcinoma: a 2017 update. *Hepatol Int* 2017; **11**: 317-370 [PMID: 28620797 DOI: 10.1007/s12072-017-9799-9]
- 4 **Viganò L**, Laurenzi A, Solbiati L, Procopio F, Cherqui D, Torzilli G. Open Liver Resection, Laparoscopic Liver Resection, and Percutaneous Thermal Ablation for Patients with Solitary Small Hepatocellular Carcinoma (≤ 30 mm): Review of the Literature and Proposal for a Therapeutic Strategy. *Dig Surg* 2018; **35**: 359-371 [PMID: 29890512 DOI:]

- 10.1159/000489836]
- 5 **Hong YJ**, Kim SH, Choi GH, Kim KS, Choi JS. Long-term outcome after liver resection and clinicopathological features in patients with small hepatocellular carcinoma. *Korean J Hepatobiliary Pancreat Surg* 2011; **15**: 199-205 [PMID: 26421040 DOI: 10.14701/kjhbps.2011.15.4.199]
 - 6 **Chen ZH**, Zhang XP, Wang H, Chai ZT, Sun JX, Guo WX, Shi J, Cheng SQ. Effect of microvascular invasion on the postoperative long-term prognosis of solitary small HCC: a systematic review and meta-analysis. *HPB (Oxford)* 2019; **21**: 935-944 [PMID: 30871805 DOI: 10.1016/j.hpb.2019.02.003]
 - 7 **Lim KC**, Chow PK, Allen JC, Chia GS, Lim M, Cheow PC, Chung AY, Ooi LL, Tan SB. Microvascular invasion is a better predictor of tumor recurrence and overall survival following surgical resection for hepatocellular carcinoma compared to the Milan criteria. *Ann Surg* 2011; **254**: 108-113 [PMID: 21527845 DOI: 10.1097/SLA.0b013e31821ad884]
 - 8 **Choi KK**, Kim SH, Choi SB, Lim JH, Choi GH, Choi JS, Kim KS. Portal venous invasion: the single most independent risk factor for immediate postoperative recurrence of hepatocellular carcinoma. *J Gastroenterol Hepatol* 2011; **26**: 1646-1651 [PMID: 21592228 DOI: 10.1111/j.1440-1746.2011.06780.x]
 - 9 **Du M**, Chen L, Zhao J, Tian F, Zeng H, Tan Y, Sun H, Zhou J, Ji Y. Microvascular invasion (MVI) is a poorer prognostic predictor for small hepatocellular carcinoma. *BMC Cancer* 2014; **14**: 38 [PMID: 24460749 DOI: 10.1186/1471-2407-14-38]
 - 10 **Zhao Y**, Zhu X, Wang H, Dong D, Gao S, Wang W. Safety and Efficacy of Transcatheter Arterial Chemoembolization Plus Radiotherapy Combined With Sorafenib in Hepatocellular Carcinoma Showing Macrovascular Invasion. *Front Oncol* 2019; **9**: 1065 [PMID: 31681599 DOI: 10.3389/fonc.2019.01065]
 - 11 **Renzulli M**, Brocchi S, Cucchetti A, Mazzotti F, Mosconi C, Sportoletti C, Brandi G, Pinna AD, Golfieri R. Can Current Preoperative Imaging Be Used to Detect Microvascular Invasion of Hepatocellular Carcinoma? *Radiology* 2016; **279**: 432-442 [PMID: 26653683 DOI: 10.1148/radiol.2015150998]
 - 12 **Rodríguez-Perálvarez M**, Luong TV, Andreana L, Meyer T, Dhillon AP, Burroughs AK. A systematic review of microvascular invasion in hepatocellular carcinoma: diagnostic and prognostic variability. *Ann Surg Oncol* 2013; **20**: 325-339 [PMID: 23149850 DOI: 10.1245/s10434-012-2513-1]
 - 13 **Golfieri R**, Renzulli M, Lucidi V, Corcioni B, Trevisani F, Bolondi L. Contribution of the hepatobiliary phase of Gd-EOB-DTPA-enhanced MRI to Dynamic MRI in the detection of hypovascular small (≤ 2 cm) HCC in cirrhosis. *Eur Radiol* 2011; **21**: 1233-1242 [PMID: 21293864 DOI: 10.1007/s00330-010-2030-1]
 - 14 **Verloh N**, Útpatel K, Zeman F, Fellner C, Schlitt HJ, Müller M, Stroszczyński C, Evert M, Wiggermann P, Haimerl M. Diagnostic performance of Gd-EOB-DTPA-enhanced MRI for evaluation of liver dysfunction: a multivariable analysis of 3T MRI sequences. *Oncotarget* 2018; **9**: 36371-36378 [PMID: 30555635 DOI: 10.18632/oncotarget.26368]
 - 15 **Huang M**, Liao B, Xu P, Cai H, Huang K, Dong Z, Xu L, Peng Z, Luo Y, Zheng K, Peng B, Li ZP, Feng ST. Prediction of Microvascular Invasion in Hepatocellular Carcinoma: Preoperative Gd-EOB-DTPA-Dynamic Enhanced MRI and Histopathological Correlation. *Contrast Media Mol Imaging* 2018; **2018**: 9674565 [PMID: 29606926 DOI: 10.1155/2018/9674565]
 - 16 **Lei Z**, Li J, Wu D, Xia Y, Wang Q, Si A, Wang K, Wan X, Lau WY, Wu M, Shen F. Nomogram for Preoperative Estimation of Microvascular Invasion Risk in Hepatitis B Virus-Related Hepatocellular Carcinoma Within the Milan Criteria. *JAMA Surg* 2016; **151**: 356-363 [PMID: 26579636 DOI: 10.1001/jamasurg.2015.4257]
 - 17 **Kaibori M**, Ishizaki M, Matsui K, Kwon AH. Predictors of microvascular invasion before hepatectomy for hepatocellular carcinoma. *J Surg Oncol* 2010; **102**: 462-468 [PMID: 20872949 DOI: 10.1002/jso.21631]
 - 18 **Suh YJ**, Kim MJ, Choi JY, Park MS, Kim KW. Preoperative prediction of the microvascular invasion of hepatocellular carcinoma with diffusion-weighted imaging. *Liver Transpl* 2012; **18**: 1171-1178 [PMID: 22767394 DOI: 10.1002/lt.23502]
 - 19 **Davnull F**, Yip CS, Ljungqvist G, Selmi M, Ng F, Sanghera B, Ganeshan B, Miles KA, Cook GJ, Goh V. Assessment of tumor heterogeneity: an emerging imaging tool for clinical practice? *Insights Imaging* 2012; **3**: 573-589 [PMID: 23093486 DOI: 10.1007/s13244-012-0196-6]
 - 20 **Aerts HJ**, Velazquez ER, Leijenaar RT, Parmar C, Grossmann P, Carvalho S, Bussink J, Monshouwer R, Haibe-Kains B, Rietveld D, Hoebers F, Rietbergen MM, Leemans CR, Dekker A, Quackenbush J, Gillies RJ, Lambin P. Decoding tumour phenotype by noninvasive imaging using a quantitative radiomics approach. *Nat Commun* 2014; **5**: 4006 [PMID: 24892406 DOI: 10.1038/ncomms5006]
 - 21 **Erickson BJ**, Korfiatis P, Akkus Z, Kline TL. Machine Learning for Medical Imaging. *Radiographics* 2017; **37**: 505-515 [PMID: 28212054 DOI: 10.1148/rg.2017160130]
 - 22 **Litjens G**, Kooi T, Bejnordi BE, Setio AAA, Ciompi F, Ghafoorian M, van der Laak JAWM, van Ginneken B, Sánchez CI. A survey on deep learning in medical image analysis. *Med Image Anal* 2017; **42**: 60-88 [PMID: 28778026 DOI: 10.1016/j.media.2017.07.005]
 - 23 **Tao Q**, Lelieveldt BPF, van der Geest RJ. Deep Learning for Quantitative Cardiac MRI. *AJR Am J Roentgenol* 2020; **214**: 529-535 [PMID: 31670597 DOI: 10.2214/AJR.19.21927]
 - 24 **Simpson AL**, Adams LB, Allen PJ, D'Angelica MI, DeMatteo RP, Fong Y, Kingham TP, Leung U, Miga MI, Parada EP, Jarnagin WR, Do RK. Texture analysis of preoperative CT images for prediction of postoperative hepatic insufficiency: a preliminary study. *J Am Coll Surg* 2015; **220**: 339-346 [PMID: 25537305 DOI: 10.1016/j.jamcollsurg.2014.11.027]
 - 25 **Li M**, Fu S, Zhu Y, Liu Z, Chen S, Lu L, Liang C. Computed tomography texture analysis to facilitate therapeutic decision making in hepatocellular carcinoma. *Oncotarget* 2016; **7**: 13248-13259 [PMID: 26910890 DOI: 10.18632/oncotarget.7467]
 - 26 **Gillies RJ**, Kinahan PE, Hricak H. Radiomics: Images Are More than Pictures, They Are Data. *Radiology* 2016; **278**: 563-577 [PMID: 26579733 DOI: 10.1148/radiol.2015151169]
 - 27 **Xu X**, Zhang HL, Liu QP, Sun SW, Zhang J, Zhu FP, Yang G, Yan X, Zhang YD, Liu XS. Radiomic analysis of contrast-enhanced CT predicts microvascular invasion and outcome in hepatocellular carcinoma. *J Hepatol* 2019; **70**: 1133-1144 [PMID: 30876945 DOI: 10.1016/j.jhep.2019.02.023]
 - 28 **Bakr S**, Echegaray S, Shah R, Kamaya A, Louie J, Napel S, Kothary N, Gevaert O. Noninvasive radiomics signature based on quantitative analysis of computed tomography images as a surrogate for microvascular invasion in hepatocellular carcinoma: a pilot study. *J Med Imaging (Bellingham)* 2017; **4**: 041303 [PMID: 28840174 DOI: 10.1117/1.JMI.4.4.041303]

- 29 **Chen Y**, Xia Y, Tolat PP, Long L, Jiang Z, Huang Z, Tang Q. Comparison of Conventional Gadoxetate Disodium-Enhanced MRI Features and Radiomics Signatures With Machine Learning for Diagnosing Microvascular Invasion. *AJR Am J Roentgenol* 2021; **216**: 1510-1520 [PMID: 33826360 DOI: 10.2214/AJR.20.23255]
- 30 **Kim SH**, Jeong WK, Kim Y, Kim MY, Kim J, Pyo JY, Oh YH. Hepatocellular carcinoma composed of two different histologic types: imaging features on gadoxetic acid-enhanced liver MRI. *Clin Mol Hepatol* 2013; **19**: 92-96 [PMID: 23593616 DOI: 10.3350/cmh.2013.19.1.92]
- 31 **Lee NK**, Kim S, Kim GH, Heo J, Seo HI, Kim TU, Kang DH. Significance of the "delayed hyperintense portal vein sign" in the hepatobiliary phase MRI obtained with Gd-EOB-DTPA. *J Magn Reson Imaging* 2012; **36**: 678-685 [PMID: 22649000 DOI: 10.1002/jmri.23700]
- 32 **van Kessel CS**, Veldhuis WB, van den Bosch MA, van Leeuwen MS. MR liver imaging with Gd-EOB-DTPA: a delay time of 10 minutes is sufficient for lesion characterisation. *Eur Radiol* 2012; **22**: 2153-2160 [PMID: 22645040 DOI: 10.1007/s00330-012-2486-2]
- 33 **Granito A**, Galassi M, Piscaglia F, Romanini L, Lucidi V, Renzulli M, Borghi A, Grazioli L, Golfieri R, Bolondi L. Impact of gadoxetic acid (Gd-EOB-DTPA)-enhanced magnetic resonance on the non-invasive diagnosis of small hepatocellular carcinoma: a prospective study. *Aliment Pharmacol Ther* 2013; **37**: 355-363 [PMID: 23199022 DOI: 10.1111/apt.12166]
- 34 **Lee S**, Kim SH, Lee JE, Sinn DH, Park CK. Preoperative gadoxetic acid-enhanced MRI for predicting microvascular invasion in patients with single hepatocellular carcinoma. *J Hepatol* 2017; **67**: 526-534 [PMID: 28483680 DOI: 10.1016/j.jhep.2017.04.024]
- 35 **Lambin P**, Leijenaar RTH, Deist TM, Peerlings J, de Jong EEC, van Timmeren J, Sanduleanu S, Larue RTHM, Even AJG, Jochems A, van Wijk Y, Woodruff H, van Soest J, Lustberg T, Roelofs E, van Elmpt W, Dekker A, Mottaghy FM, Wildberger JE, Walsh S. Radiomics: the bridge between medical imaging and personalized medicine. *Nat Rev Clin Oncol* 2017; **14**: 749-762 [PMID: 28975929 DOI: 10.1038/nrclinonc.2017.141]
- 36 **Hamerla G**, Meyer HJ, Schob S, Ginat DT, Altman A, Lim T, Gühr GA, Horvath-Rizea D, Hoffmann KT, Surov A. Comparison of machine learning classifiers for differentiation of grade 1 from higher gradings in meningioma: A multicenter radiomics study. *Magn Reson Imaging* 2019; **63**: 244-249 [PMID: 31425811 DOI: 10.1016/j.mri.2019.08.011]
- 37 **Peng J**, Zhang J, Zhang Q, Xu Y, Zhou J, Liu L. A radiomics nomogram for preoperative prediction of microvascular invasion risk in hepatitis B virus-related hepatocellular carcinoma. *Diagn Interv Radiol* 2018; **24**: 121-127 [PMID: 29770763 DOI: 10.5152/dir.2018.17467]
- 38 **Feng ST**, Jia Y, Liao B, Huang B, Zhou Q, Li X, Wei K, Chen L, Li B, Wang W, Chen S, He X, Wang H, Peng S, Chen ZB, Tang M, Chen Z, Hou Y, Peng Z, Kuang M. Preoperative prediction of microvascular invasion in hepatocellular cancer: a radiomics model using Gd-EOB-DTPA-enhanced MRI. *Eur Radiol* 2019; **29**: 4648-4659 [PMID: 30689032 DOI: 10.1007/s00330-018-5935-8]
- 39 **Taouli B**, Koh DM. Diffusion-weighted MR imaging of the liver. *Radiology* 2010; **254**: 47-66 [PMID: 20032142 DOI: 10.1148/radiol.09090021]
- 40 **Pawlik TM**, Delman KA, Vauthey JN, Nagorney DM, Ng IO, Ikai I, Yamaoka Y, Belghiti J, Lauwers GY, Poon RT, Abdalla EK. Tumor size predicts vascular invasion and histologic grade: Implications for selection of surgical treatment for hepatocellular carcinoma. *Liver Transpl* 2005; **11**: 1086-1092 [PMID: 16123959 DOI: 10.1002/Lt.20472]
- 41 **Okamura S**, Sumie S, Tonan T, Nakano M, Satani M, Shimose S, Shirono T, Iwamoto H, Aino H, Niizeki T, Tajiri N, Kuromatsu R, Okuda K, Nakashima O, Torimura T. Diffusion-weighted magnetic resonance imaging predicts malignant potential in small hepatocellular carcinoma. *Dig Liver Dis* 2016; **48**: 945-952 [PMID: 27338850 DOI: 10.1016/j.dld.2016.05.020]
- 42 **Kim JG**, Jang KM, Min GS, Kang TW, Cha DI, Ahn SH. Questionable correlation of the apparent diffusion coefficient with the histological grade and microvascular invasion in small hepatocellular carcinoma. *Clin Radiol* 2019; **74**: 406.e19-406.e27 [PMID: 30826002 DOI: 10.1016/j.crad.2019.01.019]
- 43 **Steyerberg EW**, Vergouwe Y. Towards better clinical prediction models: seven steps for development and an ABCD for validation. *Eur Heart J* 2014; **35**: 1925-1931 [PMID: 24898551 DOI: 10.1093/eurheartj/ehu207]



Published by **Baishideng Publishing Group Inc**
7041 Koll Center Parkway, Suite 160, Pleasanton, CA 94566, USA
Telephone: +1-925-3991568
E-mail: bpgoffice@wjgnet.com
Help Desk: <https://www.f6publishing.com/helpdesk>
<https://www.wjgnet.com>

